

POLARBEAR: A 28 nm FD-SOI ASIC for Decoding of Polar Codes

Pascal Giard, *Member, IEEE*, Alexios Balatsoukas-Stimming, Thomas Christoph Müller, *Student Member, IEEE*, Andrea Bonetti, *Student Member, IEEE*, Claude Thibeault, *Senior Member, IEEE*, Warren J. Gross, *Senior Member, IEEE*, Philippe Flatresse, and Andreas Burg, *Member, IEEE*

Abstract—Polar codes are a recently proposed class of block codes that provably achieve the capacity of various communication channels. They received a lot of attention as they can do so with low-complexity encoding and decoding algorithms, and they have an explicit construction. Their recent inclusion in a 5G communication standard will only spur more research. However, only a couple of ASICs featuring decoders for polar codes were fabricated, and none of them implements a list-based decoding algorithm. In this paper, we present ASIC measurement results for a fabricated 28 nm CMOS chip that implements two different decoders: the first decoder is tailored toward error-correction performance and flexibility. It supports any code rate as well as three different decoding algorithms: successive cancellation (SC), SC flip and SC list (SCL). The flexible decoder can also decode both non-systematic and systematic polar codes. The second decoder targets speed and energy efficiency. We present measurement results for the first silicon-proven SCL decoder, where its coded throughput is shown to be of 306.8 Mbps with a latency of 3.34 μ s and an energy per bit of 418.3 pJ/bit at a clock frequency of 721 MHz for a supply of 1.3 V. The energy per bit drops down to 178.1 pJ/bit with a more modest clock frequency of 308 MHz, lower throughput of 130.9 Mbps and a reduced supply voltage of 0.9 V. For the other two operating modes, the energy per bit is shown to be of approximately 95 pJ/bit. The less flexible high-throughput unrolled decoder can achieve a coded throughput of 9.2 Gbps and a latency of 628 ns for a measured energy per bit of 1.15 pJ/bit at 451 MHz.

Index Terms—polar codes, ASIC, successive cancellation, SC flip, SC list

I. INTRODUCTION

POLAR codes [1] received a lot of attention in the recent years, and they will gather even more as they have just been selected for the 5G communication standard currently under development by the 3GPP [2, p. 139]. However, to this day, only a couple of ASICs featuring decoders for polar codes have been fabricated [3], [4], making it difficult to get a good picture of what can be achieved. The chip described in [3] is for a successive-cancellation (SC) decoder that lacks the

very significant algorithmic and error-correction performance improvements that were later added to the basic SC algorithm, e.g., [5]–[7], and was fabricated on outdated technology node which does not suffer from the physical post-layout limitations of modern processes. The chip presented in [4] was built for a more recent technology but solely implements the belief-propagation decoding, an algorithm that, even compared to SC, suffers from mediocre error-correction performance at short to moderate blocklength.

Moreover, successive-cancellation list (SCL) is regarded as the most promising decoding algorithm, yet, up to now it has not been silicon proven. Successive-cancellation flip (SCF) decoding is another promising algorithm [8] for applications that can tolerate a variable decoding throughput for the benefit of superior energy efficiency. However, it has never been implemented in hardware before.

Contributions: In this paper, we present and compare two very different architectural choices for decoding of polar codes: flexible and optimized for error-correction performance versus high speed and good energy efficiency. We introduce a simple latency saving technique that is directly applicable to the SC, SCF, and SCL decoding algorithms. We describe a flexible decoder that supports any code rate for any set of frozen-bit locations as well as three different decoding algorithms with parameters that are configurable at the time of execution. Furthermore, this flexible decoder can decode both non-systematic and systematic polar codes. We present the first hardware implementation of the SCF algorithm along with its corresponding measurement results, and we show with measurement results that a dedicated fully-unrolled SC decoder offers the best energy efficiency that is almost two orders of magnitude better than a sequential list decoder. This points out the substantial cost for improving error-correction performance beyond SC decoding and for providing flexibility.

Outline: The remainder of this paper starts with Section II which provides the necessary background about polar codes along with a brief overview of the various decoding algorithms implemented on our fabricated chip. The impact on the error-correction performance of these different algorithms is also illustrated in that section. Section III describes the architecture of the POLARBEAR chip, including the hardware implementations of the two decoders with entirely orthogonal objectives featured on the chip, and the units that are necessary for the chip to function properly and to be testable. Section IV shows how the various modes of the flexible decoder compare and presents the advantages and disadvantages of each, and

Manuscript received ... The associate editor coordinating the review of this paper and approving it for publication was ...

P. Giard, A. Balatsoukas-Stimming, T. C. Müller, A. Bonetti, and A. Burg are with the Telecommunications Circuits Laboratory, École polytechnique fédérale de Lausanne, Lausanne, Vaud, Switzerland (e-mail: {pascal.giard, alexios.balatsoukas, christoph.mueller, andrea.bonetti, andreas.burg}@epfl.ch).

C. Thibeault is with the Department of Electrical Engineering, École de technologie supérieure, Montréal, Québec, Canada (e-mail: claude.thibeault@etsmtl.ca).

W. J. Gross is with the Department of Electrical and Computer Engineering, McGill University, Montréal, Québec, Canada (e-mail: warren.gross@mcgill.ca).

P. Flatresse is with STMicroelectronics, Crolles, France.

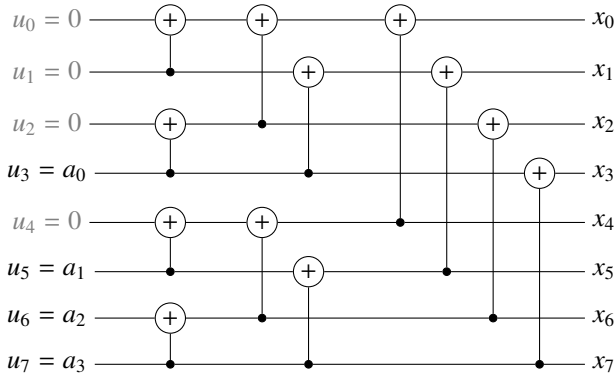


Fig. 1: Graph representation of a (8, 4) polar code.

similarly for the two architectural directions. For that purpose, detailed measurement results are presented and discussed for each decoder. A comparison against the state-of-the-art fabricated polar decoders is also carried out in that section. Finally, Section V concludes this paper.

II. POLAR CODES

A. Construction and Encoding

In his seminal work on polar codes [1], Arıkan showed that using a particular linear transformation on a vector of bits leads to a polarization phenomenon, where some of the bits become almost completely reliable when transmitted over certain types of channels while the remainder become almost completely unreliable. Polar codes exploit this phenomenon, thus provably achieving the symmetric capacity of memoryless channels as the blocklength grows to infinity.

An (N, k) polar code has a blocklength of N and rate $R = \frac{k}{N}$. It is constructed by setting the $N - k$ least reliable bits—called frozen bits—of a row vector \mathbf{u} of length N to a predetermined value, typically zero, while the remaining k locations in \mathbf{u} are used to carry the information bits a_i , $0 \leq i < k$. The set of frozen-bit indices is denoted by \mathcal{A}^c and the set of information indices is denoted by \mathcal{A} . The encoding process consists in multiplying this row vector \mathbf{u} by a $N \times N$ generator matrix $\mathbf{F}^{\otimes n}$, where $\mathbf{F}^{\otimes n}$ is recursively defined as:

$$\mathbf{F}^{\otimes n} = \begin{bmatrix} \mathbf{F}^{\otimes(n-1)} & 0 \\ 0 & \mathbf{F}^{\otimes(n-1)} \end{bmatrix} \quad (1)$$

with $\otimes n$ denoting the n -th Kronecker product of the Arıkan kernel matrix $\mathbf{F}^{\otimes 1} = \mathbf{F} = \begin{bmatrix} 1 & 0 \\ 0 & 1 \end{bmatrix}$, and $n = \log_2(N)$.

Fig. 1 illustrates the encoding process as a graph where \oplus represents a modulo-2 addition (XOR). In that representation, a polar codeword is generated by setting the frozen- and information-bit locations to 0 and a_i , $0 \leq i < k$, respectively, on the left and by propagating data through the graph from left to right. Polar codes can also be encoded systematically as described and efficiently implemented in [9] and [10], respectively. Systematic and non-systematic polar codes have the same frame-error rate (FER). In this paper, unless otherwise specified, non-systematic polar coding is used.

B. Successive-Cancellation (SC) Decoding

The SC decoding algorithm as initially proposed [1] proceeds by visiting the graph representation of Fig. 1 sequen-

tially, from right to left, from top to bottom, successively estimating $\hat{\mathbf{u}}$ from the noisy channel values. To reduce latency and increase throughput, it was first proposed to calculate two bits at once [3]. Later, the SC algorithm was further refined to use the a priori knowledge of the frozen bit locations to trim the graph [5] or even to use dedicated, and faster, decoding algorithms on parts of the graph [6]. Regardless of the version of the SC algorithm used, at all times, only one candidate codeword is considered.

C. Successive-Cancellation Flip (SCF) Decoding

The SCF decoding algorithm [8] shares many similarities with the SC algorithm. Initially, it proceeds exactly like SC decoding but while decoding it also keeps a list of the least reliable bit-decisions. Moreover it is necessary to concatenate a cyclic redundancy check (CRC) with the polar code. Once the SCF decoder has generated a complete codeword candidate, it checks if the calculated CRC matches the expected one. If the CRC check fails, then SC decoding is restarted until the bit corresponding to the least reliable bit-decision is reached. Once reached, the SCF flips that decision and resumes SC decoding. After this second round, if the calculated CRC still does not match the expected CRC, then the algorithm is rerun once more and the second least reliable bit-decision is flipped. This procedure lasts until the CRC comparison succeeds or until the maximum number of trials is reached.

D. Successive-Cancellation List (SCL) Decoding

As the name indicates, the SCL algorithm [7] also shares many similarities with the SC algorithm. Contrary to SC decoding though, the SCL decoding algorithm builds a constrained list of up to L of candidate codewords. It does so by examining both possibilities of \hat{u}_i for the locations i corresponding to information bits. A path reliability metric, calculated along the way, is used to keep only the L -best paths in the survivor list. At the very end of the decoding process, the candidate with the best path reliability metric among the L candidates is picked as the estimated codeword.

If a polar code is concatenated with a CRC, the CRC for each of the L candidates is calculated and compared against the expected one. The most reliable candidate out of all candidates that pass the CRC is selected as the decoded codeword. If all candidates fail the CRC, then the algorithm simply picks the candidate with the best path reliability metric. In this work, all SCL results use an 8-bit CRC.

E. Error-Correction Performance Comparison

Fig. 2 shows the error-correction performance of a (1024, 869) polar code for three different decoding algorithms: SC, SCL, and SCF. This particular code is used for comparison as this is also the code that is supported by the high-throughput fixed code-rate implementation of the SC algorithm. These simulation results are for random codewords modulated with binary phase-shift keying (BPSK) and transmitted over an additive white Gaussian noise (AWGN) channel. For the SCL and SCF results, the polar code is concatenated with an 8-bit CRC, i.e., the number of information bits k of the polar

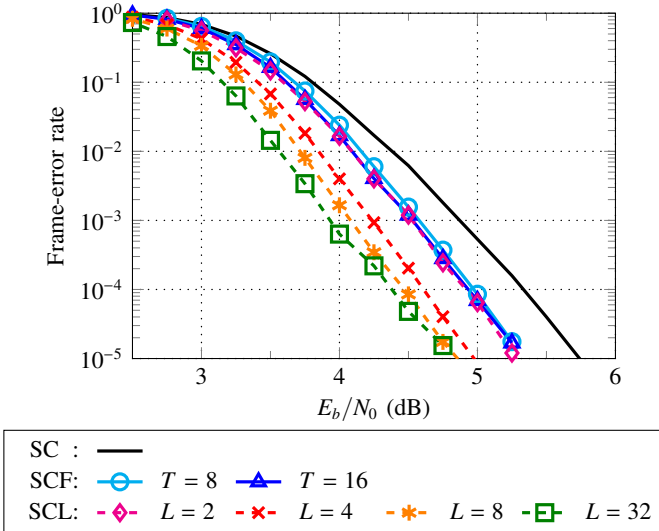


Fig. 2: Error-correction performance comparison for a (1024, 869) polar code decoded using three different algorithms. The SCL and SCF decoders use an 8-bit CRC.

code is increased by 8 such that the code rate of the resulting system remains of $R = 869/1024$. The SCF algorithm was set to do a maximum number of trials T of either 8 or 16. The list algorithm has a constrained list size L of either 2, 4, or 32. From that figure, it can be seen that the SC algorithm (black curve without markers) has the worst FER. The SCF algorithm (blue curve with triangle markers and cyan curve with circle markers) offers a coding gain from approximately 0.35 dB to 0.4 dB at a FER of 10^{-4} compared to the SC algorithm. Both SCF curves are almost identical to the SCL results with $L = 2$ (dashed-magenta curve with diamond markers). By increasing the list size L to 4 (dashed-red curve with cross markers), the SCL algorithm improves the coding gain by 0.33 dB compared to the SCF results. Further increasing the list size L to 32 (dashed-green curve with square markers) leads to a 0.31 dB gain over $L = 4$ up to a FER of approximately 10^{-3} from which point the 8-bit CRC becomes too short to avoid collisions. This causes the gain to slowly degrade as the E_b/N_0 ratio grows.

The gaps between these decoding algorithms depend on the parameters, however the order generally remains the same, i.e., SC decoding will have the worst FER of the three, while SCL decoding has the best one, and that of SCF decoding lies somewhere in between.

Fig. 3 shows the error-correction performance of polar codes of blocklength $N = 1024$, for various code rates, under SCF and SCL decoding. These FER results are included for reference as these are the codes used for the measurement results presented in Section IV.

III. POLARBEAR ARCHITECTURE

Fig. 4 shows an overview of the POLARBEAR chip architecture. POLARBEAR comprises four main units: the flexible decoder, in green, the unrolled decoder, in yellow, the clock-generation unit (CGU), in red, and the test-controller unit (TCU), made of multiple modules, all illustrated in blue with a dashed outline. Both decoders represent channel and internal soft values as quantized log-likelihood ratios (LLRs) in the 2's

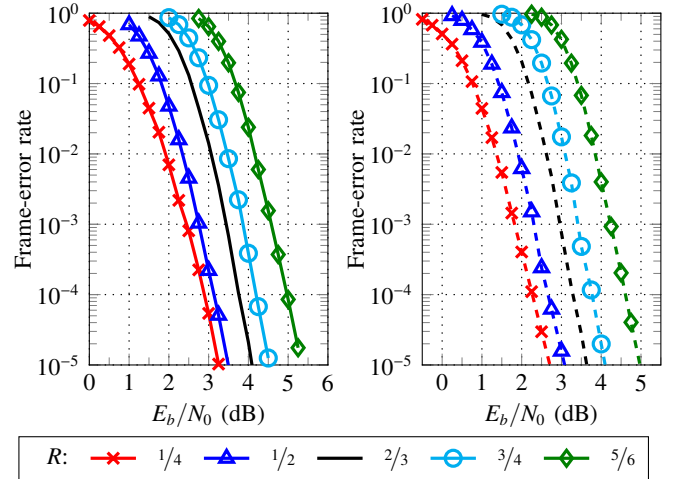


Fig. 3: Error-correction performance comparison for polar codes of blocklength $N = 1024$ with a variable code rate R decoded using either the SCF algorithm (left, solid curves) or the SCL algorithm (right, dashed curves). The SCF maximum number of trials $T = 8$, the SCL list size $L = 4$; results are for an 8-bit CRC.

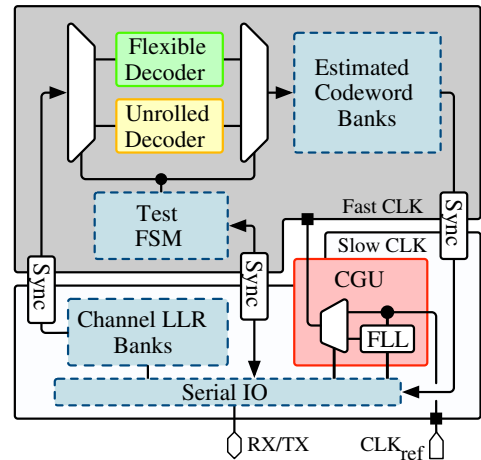


Fig. 4: Simplified overview of the POLARBEAR architecture. The Test-Controller Unit (TCU) is composed of the modules highlighted in blue with a dashed outline.

complement format. We denote quantization as $Q_i \cdot Q_c$, where Q_c is the total number of bits to store a channel LLR and Q_i is the number of bits used to store an internal LLR. Both decoders have quantization parameters that can be modified at the time of synthesis.

There are multiple power domains on the chip, supplied through distinct pins. This allows to precisely measure the current drawn by each of the two decoders.

There are two clock domains on the chip. One is slower—typically around 20 MHz—and is used as a reference clock for the CGU as well as by some of the TCU modules. The faster clock is used by the decoders, the test finite-state machine (FSM), and to read from the channel-LLR banks and to write to estimated-codeword banks. A serial interface, which is part of the TCU, provides the means to communicate with the POLARBEAR chip from the outside world. Section III-D provides a more detailed description of the TCU.

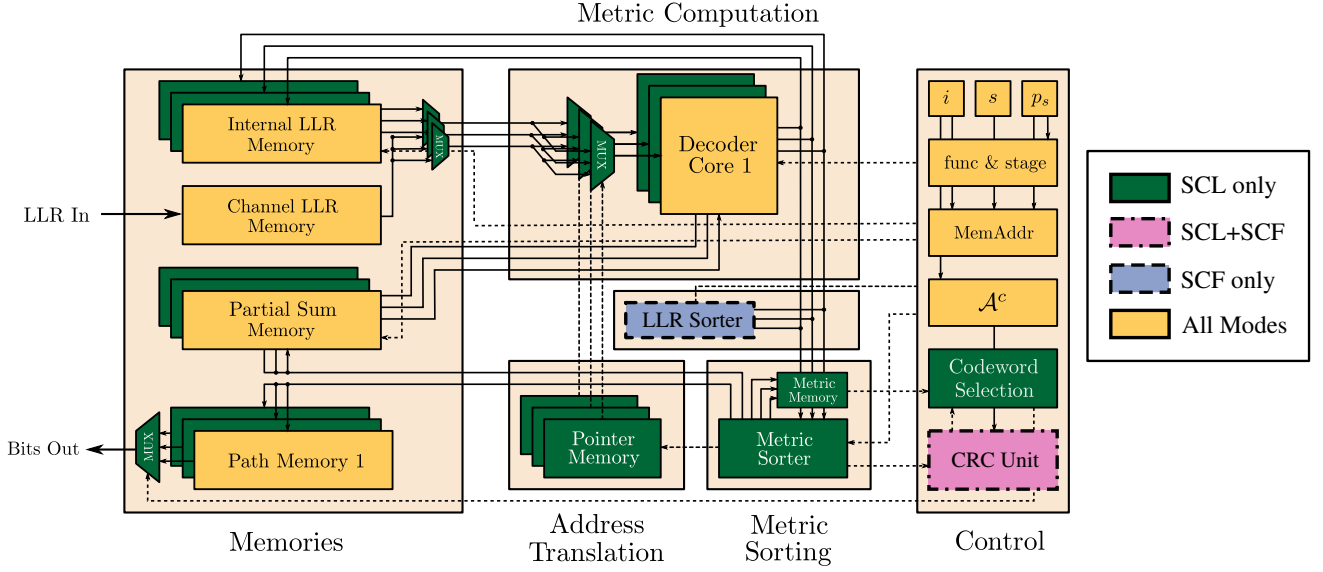


Fig. 5: Flexible-decoder architecture. In SCL decoder mode, all modules but the LLR sorter unit are used. The modules used in SCF decoder mode are colored in orange, in purple with a dashed-dotted outline, and in blue with a dashed outline. The SC mode only uses the modules colored in orange.

A. Flexible Decoder

The flexible decoder supports all three decoding algorithms described in the previous section, i.e., SC decoding, SCF decoding, and SCL decoding. This decoder also supports decoding of polar codes of any rate for a given blocklength N , various list sizes ranging from $L = 2$ up to a maximum list size $L = L_{\max}$ for SCL decoding, and a configurable maximum number of decoding trials T_{\max} for the SCF decoding algorithm. In this architecture, L_{\max} decoder cores are instantiated. Moreover, the CRC unit supports various CRC lengths in order to implement CRC-aided SCL decoding, and SCF decoding. The CRC length can be selected during runtime.

Architecture Overview: An overview of the flexible decoder architecture is presented in Fig. 5 along with a legend explaining which components are used for the different supported decoding modes.

More specifically, the decoder contains one memory bank for the channel LLRs and L_{\max} memory banks for the internal LLRs and the partial sums. Moreover, there are L_{\max} memory banks that form the path memory, which is used to store the paths taken along the decoding tree, which correspond to candidate codewords. We note that, for SC decoding of a non-systematic polar code, it is not strictly necessary to use the path memory as there is only a single candidate codeword which can be output serially as decoding proceeds. However, in our decoder architecture the single candidate codeword is stored even for SC decoding, as this enables the decoder to also decode systematic polar codes when used in conjunction with a re-encoding block to obtain the information bits. There are L_{\max} decoder cores which implement the basic update rules for SC decoding. A single decoder core is used during SC and SCF decoding, while up to L_{\max} decoder cores are used during SCL decoding, depending on the employed list size. The flexible decoder also contains two sorting units, namely the path-metric sorter (identified as “metric sorter” for short,

in Fig. 5) and the LLR sorter, which are used during SCL and SCF decoding, respectively. The path-metric sorter is used to identify the L most reliable decoding paths out of the $2L$ candidate decoding paths that are produced every time the SCL decoder encounters an information bit. We use a pruned radix- $2L$ sorter in order to sort the path metric as it is the fastest sorter for $L_{\max} = 4$ [11]. The LLR sorter, on the other hand, is used in order to identify the $T - 1$ information bits with the smallest decision-LLR absolute values, which correspond to the $T - 1$ least reliable decisions. The LLR sorter architecture is described in more detail in Section III-A3. Finally, the decoder contains a pointer memory, which implements the low-complexity state copying mechanism for SCL decoding as described in detail in [12], as well as a controller which is responsible for the generation of all control signals and for the calculation of the CRC for SCL and SCF decoding.

The set of frozen-bit locations \mathcal{A}^c is derived from a N -bit wide binary vector provided at the input, where a one or a zero indicate that the location corresponds to a frozen bit or an information bit, respectively.

Latency Saving Technique: Since the values of frozen bits are known a priori at the receiver, no LLR computations are in fact necessary until the first non-frozen bit is reached during the SC decoding process. This observation is exploited in our decoder in order to directly start decoding from the first information bit and reduce the decoding latency. Note that this latency reduction technique can be seen as partial application of the SSC algorithm [5], with the important advantage that it is applicable verbatim to SCL decoding, as the first path fork only occurs at the first information-bit location.

In the following sections, we provide more details on each of the different decoding modes.

1) *SCL Mode:* The flexible decoder implements the SCL decoding algorithm as briefly reviewed in Section II-D and as more thoroughly described in [13]. The SCL decoder imple-

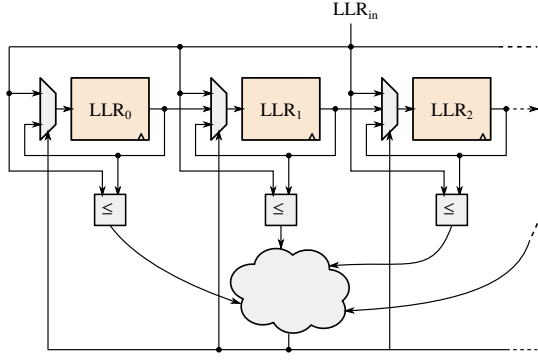


Fig. 6: Insertion sorter used in the SCF decoder to identify the $T - 1$ least reliable bit-decisions.

mentation requires all modules illustrated in Fig. 5, except for the LLR sorting unit that is only used by the SCF decoder. The CRC calculations take place alongside the decoding process, as the information bits become available one by one, and thus do not incur any additional latency. Moreover, this characteristic enables a very compact serial implementation of the CRC units, rendering their size negligible.

2) *SC Mode*: The flexible decoder also implements a slightly improved version of the original SC algorithm [1]. The improvement consists in the latency reduction technique described above, i.e., a priori knowledge of the first information-bit location allows the algorithm to skip the unnecessary calculations that would otherwise mandate the SC algorithm to visit frozen bit locations.

As illustrated in Fig. 5, the SC decoder mode only uses one of the L_{\max} decoder cores. Moreover, the SC mode uses only one of the internal-LLR-memory banks, one of the partial-sum-memory banks, and one of the path-memory banks. For SC operation both the path-metric sorting unit and the LLR sorting unit are bypassed completely.

3) *SCF Mode*: The flexible decoder also implements the SCF decoding algorithm as proposed in [8], and as briefly described in Section II-C. Similarly to the SC decoder, the SCF decoder mode only uses one of the L_{\max} decoder cores, a single internal-LLR-memory bank, a single partial-sum-memory bank, and a single path-memory bank. These components are illustrated in orange (labeled as “All Modes” in the legend) in Fig. 5. In addition to the hardware required for SC decoding, the SCF decoder uses the CRC unit, colored in purple with a dashed-dotted outline, and a dedicated LLR sorter, colored in blue with a dashed outline, that identifies the $T - 1$ least reliable bit-decisions during the first decoding attempt, i.e., the bit-decisions that had the $T - 1$ smallest absolute LLR values.

Since the decision LLRs that need to be sorted become available at a rate of at most one LLR per clock cycle, an insertion sorter was selected to implement the LLR sorter. The insertion sorter can be fully parallelized in order to sort each LLR in a single clock cycle. More specifically, each decision LLR is compared in parallel with all $T - 1$ existing (and already sorted) least reliable decision LLRs which are stored in registers. Using the result of these comparisons, it is straightforward to decide whether the new LLR should be stored and to identify the location in which it should be inserted. Insertion can then be performed efficiently in a single

clock cycle by shifting the content of the registers that are after the insertion position by one position, discarding the LLR at position $T - 1$ in the process, and writing the new LLR value in its corresponding position, while keeping the remaining contents at their place. We note that the registers containing the $T - 1$ least reliable decision LLRs are initialized to the maximum possible absolute LLR value when decoding starts. A high level block diagram of the sorter is presented in Fig. 6.

B. Decoding Latency and Throughput of the Flexible Decoder

Since all three algorithms implemented by the flexible decoder are based on SC decoding, their decoding latency is largely dictated by the decoding latency of the underlying SC hardware decoder. More specifically, the time required by the SC decoding algorithm to generate an estimated codeword, measured in clock cycles (CCs), can be expressed as:

$$\mathcal{L}_{\text{SC}} = 2N + \frac{N}{64} \log_2 \left(\frac{N}{256} \right) - \sum_{i=0}^{\log_2 N} \left\lfloor \frac{b}{2^i} \right\rfloor \left\lceil \frac{2^i}{64} \right\rceil. \quad (2)$$

where N is the polar-code blocklength, and b is the location of the first information bit. The two left-hand-side terms correspond to the latency of a semi-parallel SC decoder implementation [14], where $P = 64$. The right-hand-side term is a correction term that stems from the polar-code-specific simplifications described earlier, a contribution of this work.

The SCL algorithm performs some additional steps compared to the SC algorithm. In particular, the metric sorting step involved in SCL decoding cannot be performed in parallel with the LLR computations and thus increases the latency of the SCL decoder with respect to that of the SC decoder. More specifically, the latency of SCL decoding depends on the code rate and on the distribution of frozen-bit clusters in the polar code. Let us partition \mathcal{A}^c as $\mathcal{A}^c = \bigcup_{j=1}^{\mathcal{F}_C} \mathcal{A}_j^c$ such that:

- (i) $\mathcal{A}_j^c \cap \mathcal{A}_{j'}^c = \emptyset$ if $j \neq j'$,
- (ii) for every j , \mathcal{A}_j^c is a contiguous subset of $\{0, \dots, N - 1\}$,
- (iii) for every pair $j \neq j'$, $\mathcal{A}_j^c \cup \mathcal{A}_{j'}^c$ is not a contiguous subset of $\{0, \dots, N - 1\}$.

Then, each \mathcal{A}_j^c is a frozen-bit cluster and \mathcal{F}_C is the total number of frozen-bit clusters in a polar code.

Using the above definition of a frozen-bit cluster, the latency of the SCL decoding algorithm is given by:

$$\mathcal{L}_{\text{SCL}} = \mathcal{L}_{\text{SC}} + \mathcal{L}_{\text{sort}}, \quad (3)$$

where \mathcal{L}_{SC} is the latency of the SC decoder as defined in (2) and $\mathcal{L}_{\text{sort}}$ is the latency incurred by the sorting steps defined as [13]:

$$\mathcal{L}_{\text{sort}} = k + \mathcal{F}_C, \quad (4)$$

where k is the number of information bits and \mathcal{F}_C is the number of frozen-bit clusters. Similarly to the right-hand-side term of (2), \mathcal{F}_C is also polar-code specific.

Contrary to SC and SCL decoding, SCF decoding has a variable runtime that depends on the number of performed decoding attempts. The worst-case latency of the SCF decoding algorithm can be expressed as:

$$\mathcal{L}_{\text{SCF}} = T \mathcal{L}_{\text{SC}}, \quad (5)$$

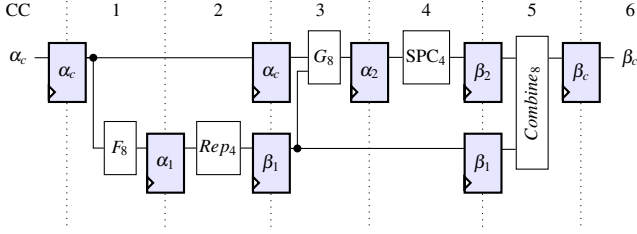


Fig. 7: Fully-unrolled partially-pipelined SC decoder architecture example for a (8, 4) polar code, where the initiation interval I equals 2. Clock gates and signals omitted for clarity.

where T is the maximum number of trials, and \mathcal{L}_{SC} is the latency of the SC decoder as defined in (2). It is noteworthy that, as will be shown in the sequel, for the FER values of interest the average latency of SCF decoding is very close to that of standard SC decoding.

Since only a single codeword is decoded at any given time by the flexible decoder, the decoding throughput can be directly calculated from the decoding latency. Thus, the coded throughput of the flexible decoder is given by:

$$\mathcal{T}_x = \frac{Nf_{\text{clk}}}{\mathcal{L}_x} \text{ bps}, \quad (6)$$

where $x \in \{\text{SC}, \text{SCF}, \text{SCL}\}$.

C. Fully-Unrolled Partially-Pipelined SC Decoder

The SC decoder implementation is optimized for speed and energy efficiency at the expense of flexibility and error-correction performance (compared to the SCL and SCF decoding algorithms), and is based on the fast-SSC algorithm [6] and on a fully-unrolled partially-pipelined architecture for a polar decoder as presented in [15].

Fig. 7 illustrates an example of a fully-unrolled partially-pipelined SC decoder for the (8,4) polar code represented as a graph in Fig. 1. Partial pipelining, as opposed to deep pipelining, allows to reduce the required area, at the cost of reducing the throughput, by removing redundant shimming registers in parts of the pipeline where data remains unchanged over multiple clock cycles [15]. In this example the initiation interval is $I = 2$, meaning that, at every second clock cycle, a new frame can be fed into the decoder and a new codeword is estimated. In Fig. 7, registers are shown in light blue, where α and β registers are for LLRs and bit-vector estimates, respectively. The blocks in white, marked F , G , $Combine$, Rep , and SPC , correspond to functions of the fast-SSC algorithm, and the subscript indicates their respective width. Data flows from left to right with very little control logic.

The latency of our unrolled decoder is polar-code specific as it depends on the distribution of the frozen bit locations [6], but it is by nature significantly smaller than \mathcal{L}_{SC} . An example of that difference is given in Table I. The coded throughput of a fully-unrolled decoder does not depend on the distribution of the frozen bit locations and is given by:

$$\mathcal{T}_{U-SC} = \frac{Nf_{\text{clk}}}{I} \text{ bps}, \quad (7)$$

where f_{clk} is the clock frequency of the decoder.

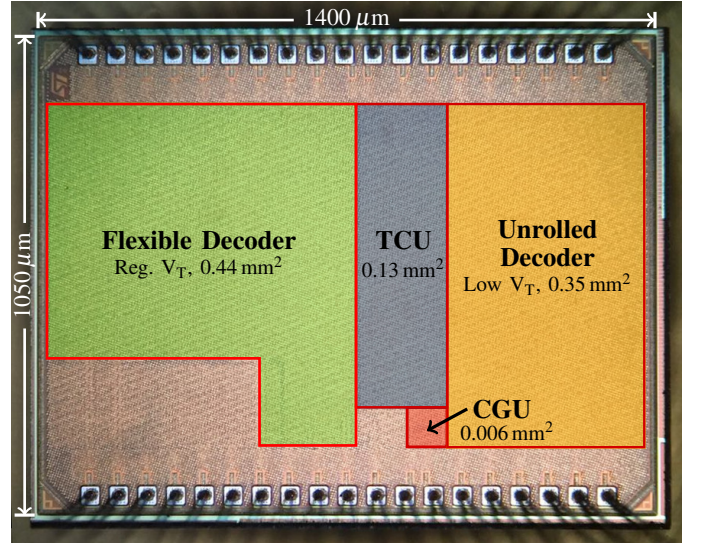


Fig. 8: POLARBEAR micrograph.

D. Clock-Generation and Test-Controller Units

The CGU, highlighted in red in Fig. 4, produces a fast clock from a reference clock by using a flexible configurable frequency lock loop (FLL) [16]. The CGU has its own supply V_{CGU} such that its energy consumption does not affect the decoder measurements.

The TCU is the interface to the decoders and the FLL. The majority of its area consists of memory, which is implemented using registers. More specifically, there are three memory banks that hold channel LLRs for three polar code frames, as well as three additional memory banks to store the corresponding estimated codewords. The TCU includes a test FSM responsible to select the desired decoder, and to configure both the FLL and the decoders. In Fig. 4, the modules composing the TCU have a dashed outline and are highlighted in blue.

The TCU uses a serial interface to communicate with the outside world. This interface implements a simple protocol that allows to read and write to a memory map. As a consequence, we can communicate with the chip from a computer, e.g. to load the channel LLRs into the banks, to read back the content of the estimated codeword banks, and to configure the FLL.

IV. TEST CHIP AND MEASUREMENT RESULTS

The POLARBEAR architecture described in Section III was fabricated in a 28 nm FD-SOI CMOS technology, where the flexible decoder uses the regular V_T flavor to minimize leakage and the unrolled decoder uses the low V_T flavor to maximize speed. The other units present on the chip all use regular V_T . The core occupies 0.93 mm² of the complete 1.47 mm² die, and has an overall density of 62%.

Fig. 8 shows a micrograph of the chip, where the area highlighted in green corresponds to the flexible decoder, the area in yellow is the fully-unrolled SC decoder, the one in blue is the TCU along with its memory, and the one in red is the CGU. The CGU can provide a clock frequency between 960 kHz and 1.275 GHz using an external reference clock of 20 MHz and a supply voltage $V_{CGU} = 0.9$ V.

TABLE I: Decoding latency in clock cycles for the various supported decoders and modes corresponding to polar codes of 5 different code rates. The unrolled decoder is denoted U-SC.

R	SC	SCL	U-SC
1/4	1577	1887	-
1/2	1833	2408	-
2/3	1896	2644	-
3/4	1960	2783	-
5/6	1991	2899	283

In the following sections, we start by describing our test setup and methodology. Then the various modes of the flexible decoder are compared against each other and against the unrolled SC decoder. Lastly our decoders are compared against the other fabricated polar decoders that can be found in the literature.

A. Test Setup and Methodology

Testing is conducted by inserting a POLARBEAR chip into a custom-made PCB which is, in turn, inserted as a daughter-board into an FPGA development board. The FPGA development board—a Xilinx XUPV5-LX110T—is connected to a PC via a serial interface. The steps to run a test can be summarized as follows:

- 1) Transfer the channel LLRs to the TCU memory.
- 2) Configure the FLL to generate the desired fast clock.
- 3) Select the desired decoder (flexible or unrolled).
If the flexible decoder was selected:
 - a) Select the desired mode.
 - b) Set the polar-code type: non-systematic or systematic.
 - c) Select the CRC length-and-polynomial pair.
 - d) Transfer the binary vector from which the set of frozen-bit indices \mathcal{A}^c is derived.
 - e) Set the index of the first information-bit location.
 - f) Set the list size L (SCL mode) or the maximum number of trials T (SCF mode).
- 4) Start the test.
- 5) Wait until the decoder notifies the TCU that decoding is complete.
- 6) Read the estimated codeword from the TCU memory.
- 7) Compare the estimated codeword against the expected one.

Measurement results are for test vectors generated using bit-true models of the decoders for an AWGN channel with an E_b/N_0 of 0 dB to obtain worst-case values, i.e., such that more switching activity is generated compared to operation in a typical E_b/N_0 region of interest. Independent programmable power supplies are used to provide power to the various cores, and a high-precision multimeter is put in the loop to measure the current drawn by the decoder of interest. Furthermore, measurements are taken in continuous decoding mode at room temperature.

For reference, the latency—in clock cycles—of the polar codes used in the measurements are provided in Table I. The latency values for the SCF mode are not included in this table as they are integer multiples of those of the SC decoder, where

TABLE II: CRC lengths and polynomials supported by the flexible decoder.

Length (bits)	Polynomial
4	$x^4 + x + 1$
8	$x^8 + x^7 + x^4 + x^2 + x + 1$
16	$x^{16} + x^{12} + x^5 + 1$

the multiplication factor is the number of trials. As it can be observed by combining equations (2), (3), and (4), the latency and throughput of the SCL mode are independent of the list size L . This is a result of having all the necessary hardware resources to accommodate the largest supported list size L_{\max} .

From Table I, it can be seen that the latency increases with the code rate. The reason for that lies in the nature of *good* polar codes where the first information bit location b is pushed further and further to the right as the code rate R decreases. As a result, the correction term of (2) increases as the code rate diminishes and the SC latency \mathcal{L}_{sc} , common to all three modes, is reduced.

B. Flexible Decoder

The flexible decoder uses the regular V_T process flavor, and occupies an area of 0.44 mm² of which 0.29 mm² are occupied by standard cells with a density of 65%. The memory, in the form of registers, accounts for 26% of the total flexible-decoder area.

1) *Quantization*: In terms of quantization, this decoder uses $Q_i \cdot Q_c$ equal to 6.6, and 8-bit path metrics for the SCL mode. Fig. 9 shows the impact of this quantization on the error-correction performance of 8-bit CRC-aided SCL decoding with $L = 4$ for polar codes of various rates. It can be seen that this quantization incurs a coding loss ranging from 0.13 dB to under 0.05 dB, at a FER of 10^{-3} , compared to using a floating-point representation. We note that the coding loss is greater for the lower-rate codes and diminishes as the rate increases.

2) *Decoding Modes*: As mentioned earlier, the flexible decoder has three operating modes corresponding to the SC, SCF, and SCL algorithms. The operating mode can be selected at execution time.

The SCL mode supports a list size L value up to $L_{\max} = 4$. As can be seen from Fig. 2, for an $N = 1024$ polar code, moving from $L = 4$ to $L = 8$ (or even $L = 32$) results in a small gain in terms of the error-correction performance for this particular code rate and we observe similar behavior for other code rates. This fact, combined with the area constraints we had for our chip, lead to the choice of $L_{\max} = 4$. Since in our architecture the configured list size L has to be a power of two, our chip supports the list sizes $L \in \{1, 2, 4\}$, where $L = 1$ is equivalent to SC mode selection. The CRC lengths supported by the decoder chip, which can be selected at the time of execution, are summarized in Table II along with the CRC polynomials that were used. These lengths were selected to cover a wide range of list sizes and rates, as different operating conditions require different CRC lengths in order to achieve the best possible performance [13]. We note that, for SCL decoding it is also possible to completely disable the CRC.

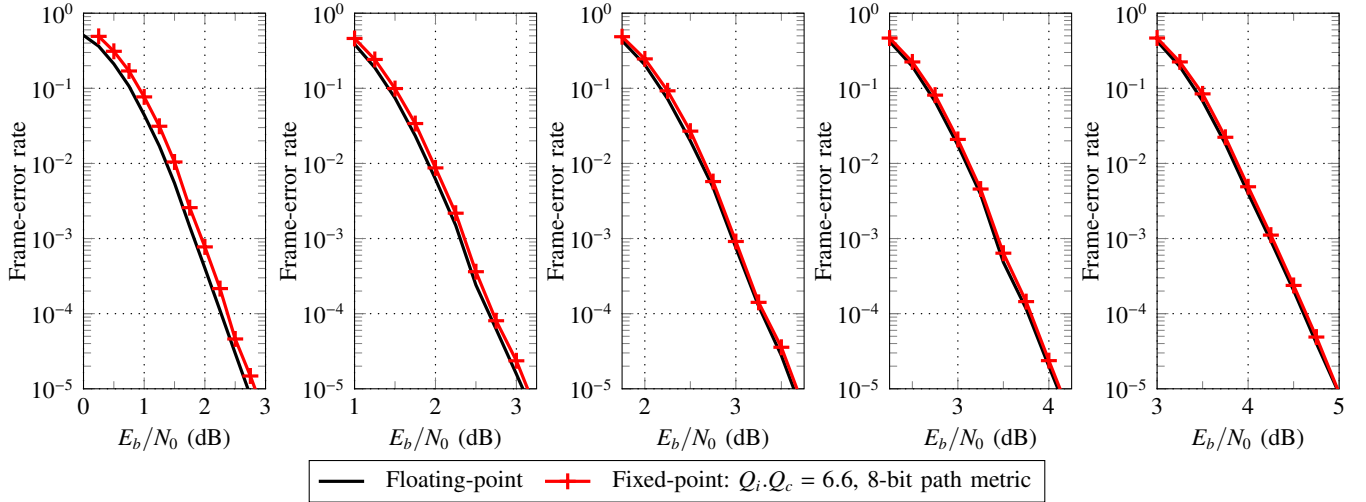


Fig. 9: Impact of LLR and path metric quantization on the error-correction performance of 8-bit CRC-aided SCL decoding with $L = 4$. From left to right, the performance of polar codes of blocklength $N = 1024$ with various code rates $R \in \{1/4, 1/2, 2/3, 3/4, 5/6\}$.

In the SCF mode, the maximum number of trials T has to be set and can have a value of up to T_{\max} . As can be seen from Fig. 2, for an $N = 1024$ polar code, moving from $T = 8$ to $T = 16$ provides very little benefit in terms of the error-correction performance. However, since increasing T_{\max} incurs a negligible hardware overhead because the LLR sorter area is very small, we decided to choose $T_{\max} = 32$ in order to ensure that we can cover a very wide range of code rate scenarios. While it is optional in the SCL mode, the SCF mode mandates activation of a CRC unit and the selection of a CRC length.

The SC mode can be selected by disabling the CRC and setting $L = 1$.

Regarding the critical path of the flexible decoder, it depends on the operating mode and parameters. In SCL mode with a list size $L = 4$, the critical path starts at the output of a register storing a path metric, goes through the metric sorter, then through a partial-sum network (PSN) (part of a decoder core), and ends at the input of the path-memory register. For the SC and SCF modes as well as the SCL mode with $L = 2$, the critical path starts from an internal-LLR memory register, goes through a processing element and into the PSN (both part of a decoder core) and ends at the input of a path-memory register.

As for any polar decoder, the flexible decoder can decode polar codes with blocklengths N smaller than 1024 by setting the 1024 - N most significant channel-LLR locations to the fixed-point equivalent of $+\infty$. However, since the controller was not optimized towards this goal, minute changes to its architecture would be required to achieve the optimal latency with no noticeable impact on area or clock frequency.

3) *Throughput Comparison*: In this section, the measured throughput and energy per bit of the three modes are compared. The 8-bit CRC is selected for the SCF and SCL modes. Since the throughput, and thus the energy per bit, of the SCF mode are highly dependent on the average number of trials, results are provided for the average number of trials required at two FER values of interest.

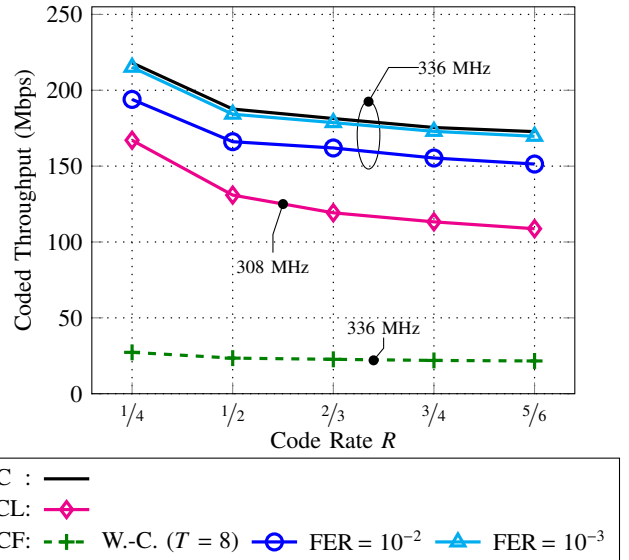


Fig. 10: Coded throughput to decode polar codes of blocklength $N = 1024$ using all three modes supported by the flexible decoder. Maximum achievable clock frequencies f_{clk} shown as annotations.

Fig. 10 shows the throughput for the three modes supported by the flexible decoder. All measurements are for the same core supply voltage of 0.9 V and for the respective maximum achievable clock frequency. Fig. 10 shows that the SC mode has a throughput that is from 31% to 59% greater than that of the SCL mode. While the worst-case (W.-C.) throughput of the SCF mode is well below that of any other mode, the achievable throughput of the SCF mode approaches that of the SC mode as the FER improves. While operating at a FER of 10^{-2} , the SCF mode is approximately 12% slower than the SC mode. This gap shrinks to under 1.5% at a FER of 10^{-3} . Comparing the SCF mode at a FER of 10^{-2} with the SCL mode, the SCF mode is from 16% to 39% faster than the SCL mode for the lowest to the highest code rates, respectively.

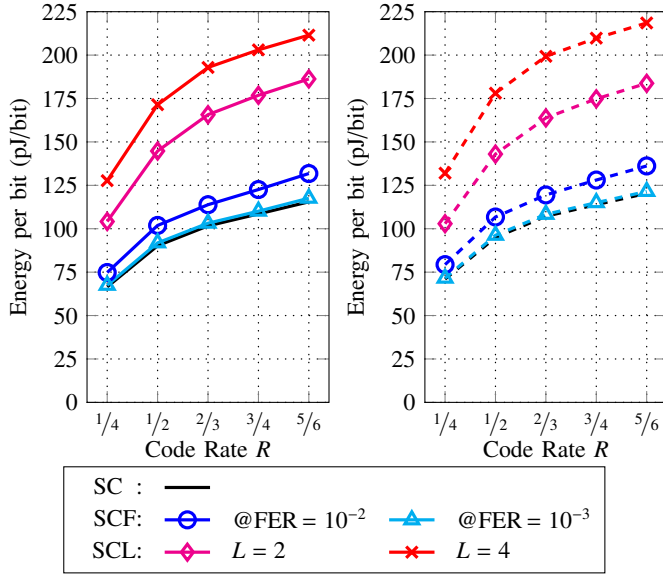


Fig. 11: Energy per bit to decode polar codes of blocklength $N = 1024$ using the various decoding algorithms supported by the flexible decoder. All measurements are for a core supply voltage of 0.9 V. Results on the left (solid curves) are for a clock $f_{\text{clk}} = 100$ MHz while the ones on the right (dashed curves) are for the respective maximum achievable clock frequency, i.e., $f_{\text{clk}} = 336$ MHz for both SC and SCF modes, and 308 MHz for the SCL mode.

4) *Energy-per-bit Comparison*: Fig. 11 shows the energy efficiency for the various modes supported by the flexible decoder. For fair comparison, all measurements are for the same core supply voltage of 0.9 V. The solid curves on the left-hand side of the figure are all for a clock frequency of $f_{\text{clk}} = 100$ MHz whereas the dashed curves on the right-hand side of the figure are for the maximum achievable clock frequencies for each decoder and mode. An 8-bit CRC is used for the SCF and SCL decoders. The energy per bit is defined as:

$$\frac{\text{Power (W)}}{\text{Coded T/P (bps)}}$$

From both sides of Fig. 11 we observe that more energy is required as the code rate increases regardless of the operating mode. This is an expected result as the latency (number of required CCs) increases with the code rate, as can be seen from Table I. The SCL mode has the greatest latency among the three modes and uses the majority of the modules of the flexible decoder illustrated in Fig. 5. Thus, as expected, Fig. 11 shows that, indeed, the SCL mode requires the most energy out of the three supported modes. From the same figure, we observe that the energy per bit of the SCF mode approaches that of the SC decoder as the FER improves (or as the E_b/N_0 ratio increases).

5) *Discussion*: With three modes that offer different characteristics, the adequate configuration can be selected at execution time according to the requirements and operating conditions. The SC mode has a constant latency, and the best throughput and energy per bit. The SCL mode, with a list size $L = 4$, requires from $1.8\times$ to $1.9\times$ more energy per bit as the SC mode, but its error-correction performance is significantly

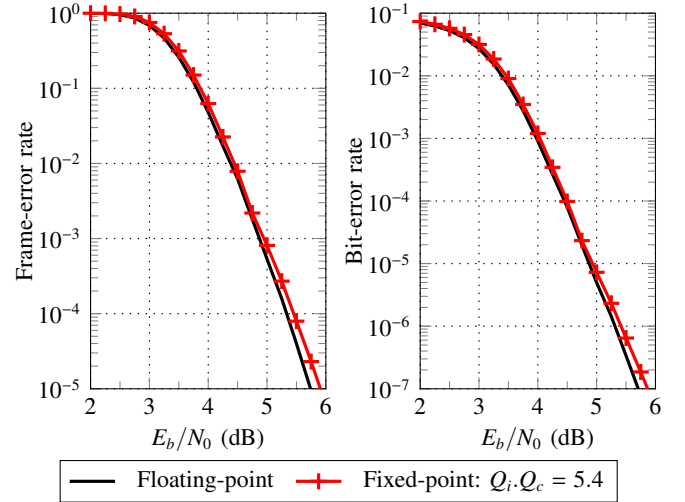


Fig. 12: Impact of LLR quantization on the error-correction performance of the systematic (1024, 869) polar code decoded by the unrolled decoder implementation.

better than that of SC. With an error-correction performance that approaches that of the SCL algorithm with $L = 2$ and an average throughput that tends to that of the SC mode as the signal-to-noise ratio improves, the SCF mode appears as the most attractive mode if the decoder is operated in a good E_b/N_0 region and if the system can cope with the variable execution time. It is interesting to note that SCL decoding with $L = 4$ does not require twice as much energy per bit than with $L = 2$. The energy-per-bit gap between the SC mode and the SCL mode with $L = 2$ is greater. The initial energy hit comes from the greater latency of SCL decoding combine with the increase in hardware resources used. Increasing L from 2 to 4, the latency remains unchanged, only the additional hardware resources used contribute to increase the energy required per bit.

C. Fully-Unrolled Partially-Pipelined SC Decoder

The unrolled decoder is implemented in the low- V_T technology flavor, and occupies an area of 0.35 mm^2 with a density of 64%. It is built for a high-rate polar code as, in many applications, the peak throughput is achieved in the best channel conditions with a high-rate code. The underlying assumption is that the unrolled decoder—implementing an SC-based algorithm that does not offer as good of an error-correction performance than SCL or SCF decoding—would only be used when the channel conditions are good. Thus, the unrolled decoder is built for a systematic (1024, 869) polar code optimized for $E_b/N_0 = 4.0$ dB, and with an initiation interval $I = 50$. It has a fixed latency of 283 CCs and uses $Q_i, Q_c = 5.4$ to represent LLRs. Fig. 12 shows that using this LLR quantization leads to a coding loss of under 0.13 dB at a FER of 10^{-4} or at a bit-error rate (BER) of 10^{-6} . To keep the longest combinational paths balanced, the dedicated decoders for the Repetition and single-parity check (SPC) codes were constrained to a maximum length of 8 and 4, respectively. The critical path starts from the output of an LLR register, goes through a dedicated decoder for a SPC code of length

TABLE III: Comparison of the flexible decoder against the other fabricated ASIC decoders for a (1024, 512) polar code. An 8-bit CRC is used for the SCF and SCL decoders.

Implementation	This work					[3]	[4]	
Algorithm	SC	SCF ($T = 8$)	SCL ($L = 4$)			SC	BP (15 iter.)	
FER @ $E_b/N_0 = 4$ dB	$\sim 1 \times 10^{-5}$	$\sim 1 \times 10^{-7}$	$\sim 7 \times 10^{-8}$			$\sim 1 \times 10^{-5}$	$\sim 7 \times 10^{-5}$	
E_b/N_0 @ FER of 10^{-5}	~ 4 dB	~ 3.4 dB	~ 3 dB			~ 4 dB	~ 4.8 dB	
Technology	28 nm	28 nm	28 nm			180 nm	65 nm	
Area (mm²)	0.44 ^a	0.44 ^a	0.44 ^a			1.71	1.48	
Supply (V)	0.9	0.9	1.3	0.9	0.5	1.3	1.0	0.475
Frequency (MHz)	336	336	721	308	20	150	300	50
Latency (CCs)	1833	14 664 (1 833 ^b)	2 408			1 568	150 (65.7 ^b)	
Latency (μs)	5.46	43.67	3.34	7.82	120.40	10.45	0.50	3.00
Coded T/P (Mbps)	187.6	187.6 ^b	306.8	130.9	8.5	98.0	4 675.8 ^{b,c}	779.3 ^{b,c}
W.-C. Coded T/P (Mbps)	187.6	23.5	306.8	130.9	8.5	98.0	2 048.0	341.3
Area Eff. (Mbps/mm²)	423	423 ^b	692	295	19	57	3,168 ^{b,c}	528 ^{b,c}
Power (mW)	17.8	17.9	128.3	23.3	0.6	67	477.5	18.6
Energy per bit (pJ/bit)	95.0	95.5 ^b	418.3	178.1	64.7	684	102.1 ^{b,c}	23.8 ^{b,c}
<i>Normalized for 28 nm and 0.9 V^o</i>								
Area (mm²)	0.44 ^a	0.44 ^a	0.44 ^a			0.04	0.27	
Frequency (MHz)	336	336	–	308	–	1 335	696	–
Latency (μs)	5.46	43.67	–	7.82	–	1.17	0.22	–
Coded T/P (Mbps)	187.6	187.6 ^b	–	130.9	–	871.9	10 847.9 ^{b,c}	–
W.-C. Coded T/P (Mbps)	187.6	23.5	–	130.9	–	871.9	4 751.4	–
Area Eff. (Mbps/mm²)	423	423 ^b	–	295	–	21 073	39 500 ^{b,c}	–
Power (mW)	17.8	17.9	–	23.3	–	5.0	166.6	–
Energy per bit (pJ/bit)	95.0	95.5 ^b	–	178.1	–	5.7	15.4 ^{b,c}	–

^aAll three modes supported by our flexible decoder occupy the same 0.44 mm².

^bAverage value at $E_b/N_0 = 4$ dB.

^cWith early-termination and an average number of iterations of 6.57.

^oArea scaled as s^2 , frequency as $1/s$, and power as v^2s , where s is the technology feature size and v is the supply voltage ratio. The frequency of [3] was first scaled back linearly to 1.8 V, the nominal voltage of the 180 nm technology.

4, and ends at the input of a bit-estimate register. Instead of using enable signals for the registers, it makes heavy use of clock gating, thus significantly reducing the area and power requirements.

In the following, the measured throughput and energy per bit are presented, and briefly discussed.

1) *Throughput and Energy-per-bit Comparisons:* The throughput of the unrolled SC decoder is over an order of magnitude greater than any of the flexible decoder modes. At a supply voltage of 0.9 V, its coded throughput is of 9 234 Mbps at an achievable clock frequency f_{clk} of 451 MHz. The energy per bit is shown to be of 2.55 pJ/bit at 100 MHz or of 1.15 pJ/bit at 451 MHz. For this decoder implemented with low- V_T cells, leakage makes for the majority of the total power consumption at 100 MHz: 3.9 mW out of 5.2 mW. At 451 MHz, the contribution of the leakage drops down to a third of the total power consumption.

2) *Discussion:* The throughput of the unrolled SC decoder is over an order of magnitude than those of the various modes supported by the flexible decoder, as presented in Fig. 10. Comparing the energy per bit of the two architectures confirms that an unrolled SC decoder built for a specific polar code can achieve the lowest energy per bit. This speed and energy-efficiency comes at the expense of flexibility.

D. Comparing with the State-of-the-Art Fabricated ASICs

Only two other fabricated ASICs can be found in the literature, both are for polar codes with a blocklength $N = 1024$. In [3], Mishra et al. presented a rate-flexible SC decoder fabricated in UMC's 180 nm CMOS technology. In [4], Park

et al. presented a rate-flexible belief-propagation (BP) decoder fabricated in TSMC's 65 nm CMOS technology. The results reported in [4] focus on a (1024, 512) polar code decoded at a high E_b/N_0 value where the average number of iterations is of 6.57 out of the maximum of 15 iterations.

Table III shows a comparison of our flexible decoder against the other fabricated ASIC decoders. We present some results for the three supported modes: SC, SCF with a maximum number of trials $T = 8$, and SCL with a list size $L = 4$. An 8-bit CRC is used for the SCF and SCL decoders. We present SCL results for three different core supply voltages. For fair comparison against [4], the table focusses on a (1024, 512) polar code decoded at a $E_b/N_0 = 4$ dB. Note that the FER at $E_b/N_0 = 4$ dB for the BP decoder was taken from [17, Fig. 4.10]—the Ph.D. thesis of the first author of [4]. The worst-case (W.-C.) coded throughput is also included as some decoding algorithms have a throughput that depends on the channel conditions. Since the results for the state of the art are for other technologies and supply voltages, normalized results are also provided for comparison.

Looking at results for the different modes of the flexible decoder, the same remarks formulated in Sections IV-B3 and IV-B4 apply when the core voltage is 0.9 V for all modes. At 0.9 V, the SC decoder shows the lowest latency and greatest throughput. Still at the same core supply, the throughput and energy efficiency of the SCF mode are on par with the SC decoder when the E_b/N_0 ratio is sufficiently high, i.e., when the number of trials becomes approximately 1. The SCL mode trails behind but still remains within the same order of magnitude.

TABLE IV: Comparison of the unrolled decoder against the other fabricated ASIC decoders for a (1024, 869) polar code.

Implementation	This work	[3]	[4]
Algorithm	SC	SC	BP (15 iter.)
E_b/N_0 @ FER of 10^{-3}	4.95	4.95	5.20
Technology	28 nm	180 nm	65 nm
Area (mm ²)	0.35	1.71	1.48
Supply (V)	0.9	1.3	1.0 0.475
Frequency (MHz)	451	150	300 50
Latency (CCs)	283	1 568	150
Latency (μ s)	0.63	10.45	0.50 3.00
W.-C. Coded T/P (Mbps)	9 233.8	98.0	2 048.0 341.3
Area Eff. (Mbps/mm ²)	26 741	57	1 384 231
Power (mW)	10.6	67	477.5 18.6
Energy per bit (pJ/bit)	1.2	684	233 54
<i>Normalized for 28 nm and 0.9 V^o</i>			
Area (mm ²)	0.35	0.04	0.27
Frequency (MHz)	451	1 335	696 –
Latency (μ s)	0.63	1.17	0.22 –
W.-C. Coded T/P (Mbps)	9 233.8	871.9	4 751.4 –
Area Eff. (Mbps/mm ²)	26 741	21 073	17 301 –
Power (mW)	10.6	5.0	166.6 –
Energy per bit (pJ/bit)	1.2	5.7	35.1 –

^oArea scaled as s^2 , frequency as $1/s$, and power as v^2s , where s is the technology feature size and v is the supply voltage ratio.

The frequency of [3] was first scaled back linearly to 1.8 V, the nominal voltage of the 180 nm technology.

Comparing our flexible decoder with the normalized results for the other works, it can be seen from Table III that the BP decoder of [4] has the lowest latency and greatest throughput while the SC decoder of [3] has the smallest area and best energy efficiency. It should be noted however that the error-correction performance of the BP decoding algorithm is significantly worse than that of any of the three algorithms supported by our flexible decoder, and that the decoder of [3] is specialized for SC decoding. Our flexible decoder is not optimized for efficient SC decoding, it implements the SC algorithm by using parts of the SCL decoder. Similarly, the area efficiency results for the SC and SCF modes are not suitable for a fair comparison against the other works as these two modes use only a fraction of the flexible decoder area, an area dictated by the largest list size supported by the SCL mode.

Table IV compares the measurement results for our dedicated unrolled decoder, specialized for one polar code, against those of the same two fabricated rate-flexible decoders [3], [4]. Note that by lack of data, and for fair comparison, we present worst-case throughput results for the BP decoder. Similarly to Table III, normalized results are presented. Comparing solely with the normalized results, it can be seen that the unrolled decoder outperforms the other works in terms of throughput and energy efficiency for an area efficiency in the same vicinity. Compared to the normalized results of the other SC decoder, the area of our decoder is approximately 10 \times greater, however the throughput is also 10 \times greater and the latency 1.8 \times lower. The area of our decoder is 1.3 \times that of the normalized area for the BP decoder, the throughput near double and the latency approximately three times greater. The energy per bit of our decoder was measured to be 4.75 \times and 29.25 \times smaller than the normalized energy-per-bit values of [3] and [4], respectively.

TABLE V: Synthesis-result comparison of SCL decoders for a (1024, 512) polar code.

Implementation	This work	[21]	[22]
List size	4	4	16
Technology	28 nm	90 nm	90 nm
Area (mm ²)	0.3	3.83	7.47
Frequency (MHz)	500	403	658
Latency (CCs)	2 408	371	1 462
Latency (μ s)	4.82	0.92	2.22
Coded T/P (Mbps)	212.6	1 112.3	460.9
Area Eff. (Mbps/mm ²)	709	290	62
<i>Normalized for 28 nm and list size $L = 4^o$</i>			
Area (mm ²)	0.3	0.4	0.2
Frequency (MHz)	500	1 295	2 115
Latency (μ s)	4.82	0.29	0.69
Coded T/P (Mbps)	213	3 575	1 481
Area Eff. (Mbps/mm ²)	709	9 645	8 195

^oArea scaled as s^2l , and frequency as $1/s$, where s is the technology feature size and l is the list-size ratio.

Further Discussion

We note that the field of polar codes has been very active since the RTL of POLARBEAR has been finalized. Many improvements were proposed to the SCL decoding algorithm and its implementation in particular. Notably, more efficient PSNs were proposed in [18], multi-bit and tree pruning methods presented [19], [20], or a combination of both, e.g. [21], [22]. These improvements are orthogonal to our work.

To help estimate the potential impact that could be brought by recent architectural improvements, Table V presents a comparison between our synthesis results for our flexible decoder (with emphasis on the SCL mode) against those from the state of the art works of [21], [22]. Normalized results, including to account for the different list size of [22], are presented.

Comparing the latency in CCs of our decoder with the other works, it can be seen that the reduced-latency algorithm of [21], that notably estimates multiple bits at once, can have a significant impact. The approximate metric sorter of [22] also leads to a latency reduction. Looking at the normalized results, it can be seen that the area results are in the same vicinity. The improved PSN of [21], [22] and the approximate sorter of [22] lead to much greater clock frequencies. By comparing the achievable clock of our synthesized design with that of our on-chip flexible decoder at 0.9 V (Table III) hints that the gains that are expected from standard scaling laws appear to be difficult to fully realize, especially with regular- V_T libraries. This is partly due to the impact of parasitics and wiring.

A detailed survey that includes the recent work and a comparison of polar decoders with low-density parity-check (LDPC) and Turbo decoders can be found in [23]. The comparison discusses, among other things, the required list size and blocklength for SCL decoding in order to match the performance of various LDPC and Turbo decoders. Another important implementation-related aspect is the quantization loss, which we showed in Section IV to be negligible when using bit-widths that are very similar to the bit-widths commonly used in LDPC decoders.

V. CONCLUSION

In this paper, we presented measurement results for POLARBEAR, a fabricated chip in 28 nm FD-SOI CMOS technology that implements two decoders for polar codes. The first decoder is flexible, supporting three different modes corresponding to distinct decoding algorithms: SC, SCF and SCL. It implements a latency saving technique applicable to all three decoding algorithms. Furthermore, this flexible decoder can decode both non-systematic and systematic polar codes of any code rate. The list size and maximum number of trials for SCL and SCF decoding modes, respectively, are configured at execution time. The second decoder is a fully-unrolled partially-pipelined SC decoder built for speed. To our knowledge, this paper presents the first ASIC measurement results for both the SCF and SCL algorithms.

We presented a flexible decoder where the most suitable mode can be selected at execution based on the requirements and operating conditions. The SC mode was shown to have the best throughput and energy per bit. For the best error-correction performance, the SCL mode was shown to be the most favorable choice at the expense of a greater energy per bit compared to both the SC and SCF modes. Lastly, with an error-correction performance that approaches that of the SCL algorithm with $L = 2$ and an average throughput that tends to that of the SC mode as the signal-to-noise ratio improves, the SCF mode appeared as the most attractive mode if the decoder is operated in a good E_b/N_0 region and if the system can cope with a variable execution time.

In terms of more specific results, we showed that in the SCL mode, our flexible decoder could achieve a coded throughput of 306.8 Mbps with a latency of $3.34 \mu\text{s}$ and an energy per bit of 418.3 pJ/bit at a clock frequency of 721 MHz for a supply of 1.3 V. The energy efficiency was shown to improve twofold with the energy per bit dropping down to 178.1 pJ/bit with the more modest clock frequency of 308 MHz, throughput of 130.9 Mbps, and supply voltage of 0.9 V. In the other two operating modes, our measurement results showed that our flexible decoder had an energy per bit of approximately 95 pJ/bit with a core supply voltage of 0.9 V. It should be noted that research on SCL decoding has been moving quickly since this chip has been sent out for tapeout. This makes us confident that ASIC results can only improve from here if all the latest improvements from the recent literature are to be incorporated.

The unrolled decoder was shown to be capable of achieving an area efficiency of $26.74 \text{ Gbps}/\text{mm}^2$ at 451 MHz for a supply voltage of 0.9 V and an energy per bit of 1.15 pJ/bit. These results confirmed that a specialized unrolled polar decoder has significantly better energy per bit and speed than its flexible counterpart. When it comes to the energy-efficiency advantage, the key ingredients were the polar code-specific specialization, the unrolling, and the use of clock gating. Since the design of this chip, it was shown in [15] that such a decoder can be made to support multiple codes of various rates and blocklengths.

ACKNOWLEDGEMENT

The authors would like to thank Christian Senning and Lorenz Schmid (formerly EPFL) for their support, Ivan Miro-Padanés (CEA-LETI) for providing the FLL [16] along with

support for it, and Marc-André Carbonneau (ÉTS) for the test PCB design. Furthermore, we would like to thank STMicroelectronics for chip fabrication.

REFERENCES

- [1] E. Arıkan, "Channel polarization: A method for constructing capacity-achieving codes for symmetric binary-input memoryless channels," *IEEE Trans. Inf. Theory*, vol. 55, no. 7, pp. 3051–3073, Jun 2009.
- [2] MCC Support, "Final Report of 3GPP TSG RAN WG1 #87 v1.0.0," Feb 2017. [Online]. Available: http://www.3gpp.org/ftp/tsg_ran/WG1_RL1/TSGR1_88/Docs/R1-1701552.zip
- [3] A. Mishra, A. J. Raymond, L. Amaru, G. Sarkis, C. Leroux, P. Meinerzhagen, A. Burg, and W. J. Gross, "A successive cancellation decoder ASIC for a 1024-bit polar code in 180nm CMOS," in *IEEE Asian Solid State Circuits Conf. (A-SSCC)*, Nov 2012, pp. 205–208.
- [4] Y. S. Park, Y. Tao, S. Sun, and Z. Zhang, "A 4.68Gb/s belief propagation polar decoder with bit-splitting register file," in *Symp. on VLSI Circuits Dig. of Tech. Papers*, Jun 2014, pp. 1–2.
- [5] A. Alamdar-Yazdi and F. R. Kschischang, "A simplified successive-cancellation decoder for polar codes," *IEEE Commun. Lett.*, vol. 15, no. 12, pp. 1378–1380, Oct 2011.
- [6] G. Sarkis, P. Giard, A. Vardy, C. Thibeault, and W. J. Gross, "Fast polar decoders: Algorithm and implementation," *IEEE J. Sel. Areas Commun.*, vol. 32, no. 5, pp. 946–957, May 2014.
- [7] I. Tal and A. Vardy, "List decoding of polar codes," *IEEE Trans. Inf. Theory*, vol. 61, no. 5, pp. 2213–2226, May 2015.
- [8] O. Afisiadis, A. Balatsoukas-Stimming, and A. Burg, "A low-complexity improved successive cancellation decoder for polar codes," in *Asilomar Conf. on Signals, Syst. and Computers*, Nov 2014, pp. 2116–2120.
- [9] E. Arıkan, "Systematic polar coding," *IEEE Commun. Lett.*, vol. 15, no. 8, pp. 860–862, Jun 2011.
- [10] G. Sarkis, I. Tal, P. Giard, A. Vardy, C. Thibeault, and W. J. Gross, "Flexible and low-complexity encoding and decoding of systematic polar codes," *IEEE Trans. Commun.*, vol. 64, no. 7, pp. 2732–2745, Jul 2016.
- [11] A. Balatsoukas-Stimming, M. Bastani Parizi, and A. Burg, "On metric sorting for successive cancellation list decoding of polar codes," in *IEEE Int. Symp. on Circuits and Syst. (ISCAS)*, May 2015, pp. 1993–1996.
- [12] A. Balatsoukas-Stimming, A. J. Raymond, W. J. Gross, and A. Burg, "Hardware architecture for list successive cancellation decoding of polar codes," *IEEE Trans. Circuits Syst. II*, vol. 61, no. 8, pp. 609–613, Aug 2014.
- [13] A. Balatsoukas-Stimming, M. Bastani Parizi, and A. Burg, "LLR-based successive cancellation list decoding of polar codes," *IEEE Trans. Signal Process.*, vol. 63, no. 19, pp. 5165–5179, Oct 2015.
- [14] C. Leroux, A. Raymond, G. Sarkis, and W. J. Gross, "A semi-parallel successive-cancellation decoder for polar codes," *IEEE Trans. Signal Process.*, vol. 61, no. 2, pp. 289–299, Jan 2013.
- [15] P. Giard, G. Sarkis, C. Thibeault, and W. J. Gross, "Multi-mode unrolled hardware architectures for polar decoders," *IEEE Trans. Circuits Syst. I*, vol. 63, no. 9, pp. 1443–1453, Aug 2016.
- [16] I. Miro-Panades, E. Beigné, Y. Thonnart, L. Alacoque, P. Vivet, S. Lesecq, D. Puschini, A. Molnos, F. Thabet, B. Tain, K. B. Chehida, S. Engels, R. Wilson, and D. Fuin, "A fine-grain variation-aware dynamic Vdd-hopping AVFS architecture on a 32 nm GALS MPSoC," *IEEE J. Solid-State Circuits*, vol. 49, no. 7, pp. 1475–1486, Jul 2014.
- [17] Y. S. Park, "Energy-efficient decoders of near-capacity channel codes," Ph.D. dissertation, University of Michigan, 2014.
- [18] Y. Fan and C.-Y. Tsui, "An efficient partial-sum network architecture for semi-parallel polar codes decoder implementation," *IEEE Trans. Signal Process.*, vol. 62, no. 12, Apr 2014.
- [19] G. Sarkis, P. Giard, A. Vardy, C. Thibeault, and W. J. Gross, "Fast list decoders for polar codes," *IEEE J. Sel. Areas Commun. - Special Issue on Recent Advances In Capacity Approaching Codes*, vol. 34, no. 2, pp. 318–328, Feb 2016.
- [20] B. Yuan and K. K. Parhi, "Low-latency successive-cancellation list decoders for polar codes with multibit decision," *IEEE Trans. VLSI Syst.*, vol. 23, no. 10, pp. 2268–2280, Oct 2015.
- [21] J. Lin, C. Xiong, and Z. Yan, "A high throughput list decoder architecture for polar codes," *IEEE Trans. VLSI Syst.*, vol. 24, no. 6, Jun 2016.
- [22] Y. Fan, C. Xia, J. Chen, C. Y. Tsui, J. Jin, H. Shen, and B. Li, "A low-latency list successive-cancellation decoding implementation for polar codes," *IEEE J. Sel. Areas Commun.*, vol. 34, no. 2, pp. 303–317, Feb 2016.
- [23] A. Balatsoukas-Stimming, P. Giard, and A. Burg, "A comparison of polar decoders with existing LDPC and turbo decoders," in *IEEE Wireless Commun. and Netw. Conf. (WCNC)*, Mar 2017, pp. 1–6.